Copolymers Based on Epoxidized Soy Bean Oil and Diglycidyl Ether of Bisphenol A: Relation Between Morphology and Fracture Behavior

AQ1 **F.I. Altuna,[1] V. Pettarin,[1] L. Martin,[2] A Retegi,[2] I. Mondragon,[2] R.A. Ruseckaite,[1] P.M. Stefani[1]**

[1] *Research Institute of Material Science and Technology (INTEMA), National Research Council (CONICET),*
AQ2 *National University of Mar del Plata (UNMdP), Juan B. Justo 4302, B7608FDQ Mar del Plata, Argentina*

[2] *Dpto. Ingeniería Química y M. Ambiente, Materials + Technologies' Group, Escuela Politécnica, Universidad País Vasco/Euskal Herriko Unibertsitatea, Pza. Europa 1, 20018 Donostia-San Sebastián, Spain*

Epoxidized soybean oil (ESO) was proved to be a good alternative to partially replace a synthetic commercial epoxy resin in a formulation to obtain thermosetting polymer, contributing to transform a vegetable oil into a higher added value product. This work focuses on the study of the fracture behavior of copolymers based on anhydride-cured epoxy systems with different contents of ESO as a replacement for the synthetic resin. It was found that fracture toughness was greatly improved when replacing diglycidyl ether of bisphenol A (DGEBA) by ESO, being the critical stress intensity factor (K_{IC}) 1.067 MPa·m$^{1/2}$ for cured ESO and 0.557 MPa·m$^{1/2}$ for cured DGEBA. The better performance of ESO networks was ascribed to its higher ability to attain plastic deformation. Moreover, for DGEBA-ESO systems, the morphologies generated during the curing process were also considered to account for the observed results. POLYM. ENG. SCI., 00:000–000, 2013.

INTRODUCTION

Over the last few decades, the increasing concern about the negative impact on the environment of the massive use of fossil sources as energy and raw materials supply has attracted increasing interest on the exploitation of renewable resources as a potential substitute. In this context, the utilization of materials derived from the biomass has been extensively studied as an alternative to the petroleum based feedstock in the production of polymeric materials [1–4]. This tendency is clearly reflected in recent market analysis: bioplastics cover approximately 10–15% of the total plastics market and it is expected to continue increasing its market share in the next years [4, 5]. Vegetable oils, in particular, constitute one of the most abundant and readily accessible biogenic materials, and its use in thermosetting polymers formulations has been explored [6–9].

One of the industrially important vegetable oil is that obtained from soybean grains. More than 80% of the world soybean production is concentrated in South and North America, Argentina being the third largest soybean producer behind the United States and Brazil [10]. Therefore, the use of soybean oil instead of synthetic resins in higher added value products would be not only of environmental but also of social and economical importance.

Soybean oil, as most vegetable oils, is characterized by its low reactivity; hence some chemical modifications are needed to overcome this limitation. Wool and coworkers have summarized many pathways to obtain functionalized vegetable oils which can be used with a wide variety of reagents to obtain thermosetting polymers [1, 11]. One of these methods involves the oxidation of the double bonds, which can be performed by chemical [12], or enzymatic route [13–15], yielding an epoxidized vegetable oil (EVO). Nowadays epoxidized soybean oil (ESO) is commercially available, as it is frequently used as a plasticizer for poly(vinyl chloride) (PVC) [16].

The use of ESO as potential partial or total substitute of commercial epoxy prepolymers has been quoted in the literature [6, 17–20]. Nevertheless, scarce information about the fracture behavior of such systems is currently available, even though it constitutes a key aspect

Correspondence to: P.M. Stefani; e-mail: pmstefan@fi.mdp.edu.ar
Contract grant sponsor: National Research Council, Argentina (CONICET); contract grant number: PIP 112-200801-01837; contract grant sponsor: National Agency of Scientific and Technological Promotion (ANPCyT); contract grant number: PICT 2006-01560; contract grant sponsor: National University of Mar del Plata.
DOI 10.1002/pen.23588
Published online in Wiley Online Library (wileyonlinelibrary.com).

that must be considered for their end-use applications, taking into account that epoxy polymers are inherently brittle [21].

A number of methods have been proposed to improve their toughness. One of the most effective involves the modification of the uncured system with an initially miscible liquid elastomer that can phase-separate during the curing of the system. Several authors have studied the toughening effect of using EVOs as liquid rubbers to modify epoxy systems. Ratna [22] analyzed the impact properties of an epoxy resin with 0–30 wt% ESO, and compared a one-stage and a two-stage processes to obtain the cured networks. The two-stage process gave place to a biphasic structure which led to a significant improvement of the impact strength, but only a minor improvement was observed for the one-stage processed networks which showed a single phase morphology. An interesting option is to use the EVOs as a reactive modifier to improve the epoxy network toughness, and this alternative was explored by Miyagawa et al. [19]. The authors evaluated the fracture behavior of anhydride cured epoxy networks modified with ESO or epoxidized linseed oil (ELO). They found that the fracture toughness showed no significant change with the addition of ELO, but it was greatly improved with the addition of 30 wt% ESO, and they ascribed this behavior to the biphasic structure developed in the latter case. To a similar conclusion arrived Park and coworkers [18, 23], by studying the fracture toughness of mixtures of synthetic epoxy prepolymers and ESO or epoxidized castor oil (ECO) cured with a thermally latent initiator. The addition of ESO to a tetrafunctional epoxy prepolymer resulted in a biphasic structure, which led to an increased toughness. The use of ECO was also found to improve the fracture properties of the epoxy polymers, though no disperse phase was observed in this case, and the improvement of the toughness was ascribed to the lower crosslinking density of the modified networks.

Beside the morphology, other factors play an important role on the fracture properties of epoxy resins. Arias et al. [24] demonstrated that the ability of the matrix to promote plastic deformation (yield stress) represents an important contribution to the toughness. The yield stress is related to the network structure, and particularly with some characteristics such as the crosslink density and the chains flexibility, and consequently these parameters must also be accounted to explain the mechanisms involved in the toughening of an epoxy matrix.

The aim of this work was to study the fracture behavior of anhydride-cured epoxy systems, and to establish the fracture mechanisms developed for different ESO contents.

The fracture toughness of the different cured formulations was measured, and the results were analyzed on the basis of the mechanical properties previously determined [20], the morphologies developed during the curing reaction, which were observed by atomic force microscopic techniques, and the mechanical properties of each phase, as determined by depth-sensing indentation.

EXPERIMENTAL

Materials

The epoxy prepolymer was a commercial grade diglycidyl ether of bisphenol A (DGEBA, Araldite GY250; Distraltec, Buenos Aires, Argentina) with epoxide equivalent weight (EEW) = 185 g/equiv. ESO (iodine value = 2.4 and EEW = 241 g/equiv., average molecular weight = 940 g/mol), was kindly supplied by Unipox S. A. (Buenos Aires, Argentina). Both chemicals, DGEBA and ESO, were dried at 70°C under vacuum during 12 h before use. The hardener methyl tetrahydrophtalic anhydride (MTHPA) (>99%, equivalent weight = 166 g/equiv.) was obtained from Distraltec (Buenos Aires, Argentina). 1-methyl imidazole (1MI) (>99%) was purchased from Huntsman (Buenos Aires, Argentina) and was used as received. The chemical structures of DGEBA, ESO, MTHPA, and 1MI are shown in Fig. 1. F1

Synthesis of the DGEBA–ESO Networks

ESO was used to replace 20, 40, 60, 80, and 100 wt% of the DGEBA in the resin formulations. Blending was performed in a one-stage process by the direct mixing of epoxy precursors with a stoichiometric amount of MTHPA and a 1MI (3 wt% on the basis of the anhydride weight). All formulations were manufactured in accordance with the procedure reported elsewhere [20]. Basically, all formulations were placed in a glass round-bottom flask and heated at 50°C for 30 min. The mixing process was carried out under reduced pressure (~10 mm Hg) to minimize the volume of air bubbles entrapped in the bulk. Subsequently, the reactive mixtures were cast into the mold at room temperature and placed inside a programmable oven (Yamato DKN400) using a two-step curing cycle: 130°C for 1 h and then 190°C for 3 h [20]. Finally, the specimens were cut into suitable dimensions for mechanical tests.

AFM

The morphology of the cured systems was studied by atomic force microscopy (AFM). It was carried out on samples of approximately 1 mm^2, obtained by cutting a proper section of the specimens with an ultramicrotome Leica Ultracut UCT (Wetzlar, Germany). A scanning probe microscope (SPM) Nanoscope III Multimode, from Digital Instruments (Santa Bárbara) was used, operating in tapping mode and using silicon cantilevers with a resonance frequency of 200–400 kHz and a spring constant of 13–102 N/m.

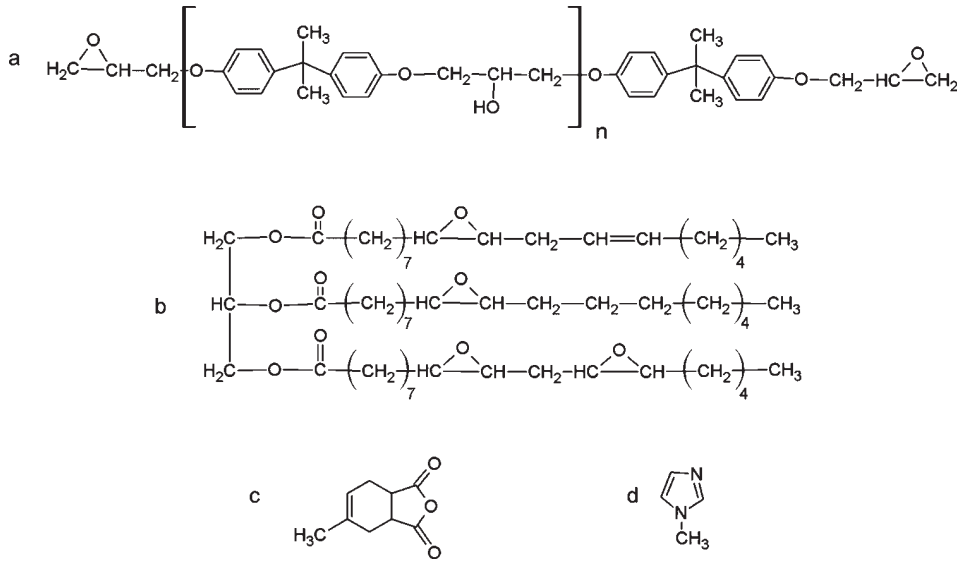

FIG. 1. Chemical structures of the reactives. (a) DGEBA, $n = 0.109$; (b) ESO; (c) MTHPA; (d) 1MI.

Fracture Tests

The fracture toughness of the cured samples was assessed using the linear elastic fracture mechanics approach to determine the critical stress intensity factor in plane strain, K_{IC} [21]. Single edge notched (SEN) specimens ($7 \times 13 \times 60$ mm^3) were prepared by notching at the center of the sample with a reciprocating saw, and subsequently by carefully tapping on a new razor blade placed in the notch to initiate a sharp crack (Fig. 2a). The specimens were tested in an Instron 4467 (Buckinghamshire, United Kingdom) universal testing machine in a three-point bending mode, at a crosshead speed of 2.0 mm/min, according to ASTM D 5045-99. From load-displacement plots of the SEN specimens and known crack lengths, the following expression was used to calculate the stress intensity factor K_{IC}:

$$K_{IC} = \frac{f(a/W)P}{BW^{1/2}} \quad (1)$$

where P is the maximum load from the load-displacement trace, expressed in kN, B is the thickness of the specimen, a is the crack length, W is the specimen height (B, a, and W must be used in cm), $f(a/W)$ is a dimensionless function of the ratio a/W given by ASTM D5045-99 standard and K_{IC} is given in units of MPa·m$^{1/2}$. It was verified that all the samples meet the criteria established by the ASTM 5045-99 standard to be considered as a valid K_{IC} value. To this purpose, the values of yield strength reported in a previous work[17] were used. The mean value of at least 10 samples per ESO content was reported as K_{IC}. Analysis of variance (ANOVA) was used ($\alpha = 0.05$), and the Tukey test was applied to identify which groups were significantly different from the others ($p < 0.05$).

To analyze the damage zone around the crack tip, the double-notch four-point-bend (DN-4PB) technique was used (Fig. 2b) following a procedure previously described in the literature [24]. Two edge cracks of approximately equal length were generated in the specimen ($7 \times 13 \times 60$ mm^3) following the same procedure explained above for K_{IC} test. The specimen was then loaded in a four-point bending fixture at a crosshead speed of 2.0 mm/min, locating the two precracks within the minor span on the tensile side. Owing to stress intensification at the crack tips, a plastic zone formed independently at each crack tip upon loading (the precrack spacing exceeded the size of the plastic zone). Because the precracks were not iden-

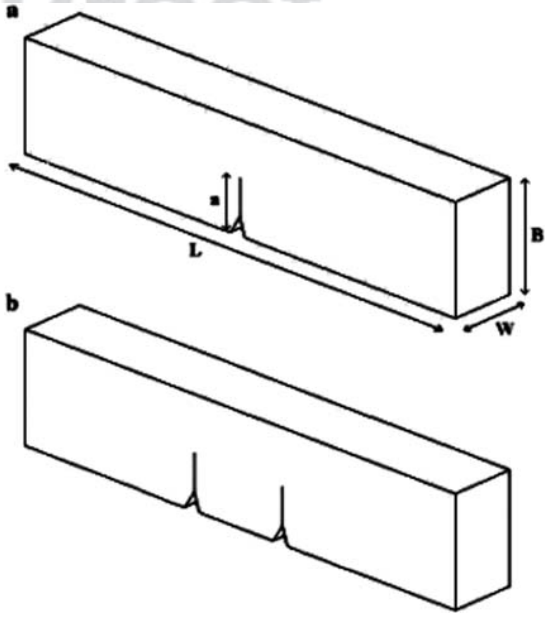

FIG. 2. Scheme of the SEN (a) and DN-4PB (b) specimens used.

tical, one of them eventually became critical and propagated in an unstable manner, thus unloading the other crack that was immediately arrested.

The damage zones around the surviving crack tips were examined by transmission optical microscopy (TOM). Thin sections were obtained using a conventional polishing technique [24, 25]. Blocks containing the surviving crack tips were cut from the samples, in a normal section to the fracture surface, but parallel respect to the crack growing direction. The blocks were then encapsulated in an epoxy formulation that was allowed to cure at room temperature. Excess material was cut using a diamond saw and the sample was polished again until it reaches a thicknesses in the range between 200 and 300 μm. Optical micrographs were recorded using a transmission microscope Leica DMLB (Wetzlar, Germany), with and without cross polarizers.

The surviving crack tips zones of the specimens were furthermore studied by AFM as was before described.

Depth-Sensing Indentation

Depth-sensing indentation tests, performed on the continuous and disperse phase of the 40 and 60% ESO samples, were used to compare the properties of each phase. Samples were prepared using the same polishing tech-

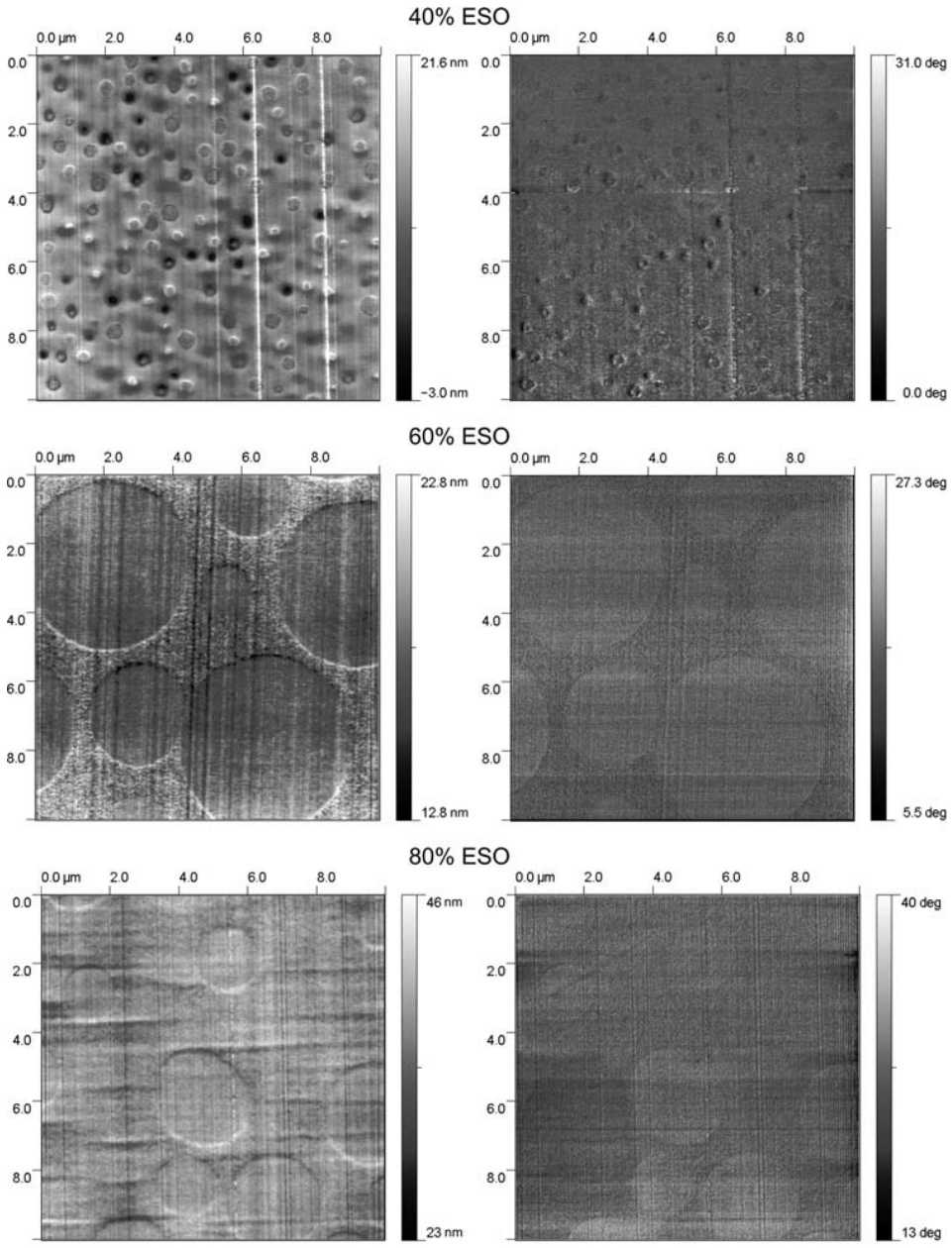

FIG. 3. AFM images of the cured samples with 40, 60, and 80% ESO. Height (left) and phase (right) images. [Color figure can be viewed in the online issue, which is available at wileyonlinelibrary.com.]

AQ5

ID: kothandamk Date: 19/3/13 Time: 20:15 Path: N:/3B2/PEN#/Vol00000/130093/APPfile/JW-PEN#130093

nique that for the TOM samples. Tests were carried on a Triboindenter (Hysitron) at room temperature using 60° three-sided pyramidal tip. Experiments involved complete loading–holding–unloading cycles under displacement controlled conditions (trapezoidal displacement functions). Depths of 200 nm for the 40% ESO samples, and 400 nm for 60% ESO samples were used, with a holding time of 5 s in both cases. Surface images were obtained using the in situ Scanning Probe Microscopy (SPM) imaging, in order to assign the obtained curves to the corresponding phase.

Optical Properties

Optical transmission was evaluated on 150–170-μm thick samples cured between glasses, using a UV–visible spectrophotometer Agilent 8453 (Palo Alto). The transmittance percentage was followed for wavelengths (λ) in the range of 300–800 nm, and for the sake of comparison the average transmittance in the wavelength range used was evaluated for each system.

RESULTS AND DISCUSSION

Thermal and Mechanical Properties

The analysis of the thermal and mechanical properties of the DGEBA-ESO/MTHPA copolymers, reported elsewhere [20], showed a decrease in the glass transition temperature (T_g) values and in the mechanical properties when more than 20% of the DGEBA was replaced by ESO. According to those results, the highest T_g value was observed for pure DGEBA/MTHPA/1MI, and values reduced with increasing ESO content. In general, T_g, as well as the yield strength (σ_y), depend not only on crosslinking density but also on polymeric chains flexibility, and therefore T_g and σ_y values are closely related [24]. In the present case, the crosslinking density (v) of DGEBA/MTHPA and ESO/MTHPA pure systems was estimated using the following equation, derived from the rubber elasticity theory:

$$E' = 3RTv \tag{2}$$

where R is the universal gas constant, T the absolute temperature and E' is the storage modulus at $T_g + 30°C$ measured by DMA and reported elsewhere [20]. Estimated v values were 1820 and 2000 mol/m^3 for DGEBA/MTHPA and ESO/MTHPA networks respectively, revealing that differences in T_g values could not be attributed to disparity in the crosslinking density. Therefore the decrease of the T_g values (and σ_y values) with the progressive replacement of DGEBA by ESO could be more likely associated with a reduced contribution of the aromatic phenyl groups of DGEBA, which confer stiffness to the polymeric chains.

Morphology Analysis

One of the main factors in determining the fracture behavior of a formulation, besides the yield strength, is the morphology. Therefore, a deep elucidation of this issue is mandatory. Particularly, the copolymers with ESO contents from 40 to 80% underwent phase separation when curing under the conditions used herein, due to differences in DGEBA and ESO reactivity with MTHPA, as it was demonstrated by scanning electron microscopy elsewhere [20]. A more clear insight of the copolymers morphology can be obtained using AFM images (Fig. 3). F3 An important difference between 40% ESO sample on one side, and 60 and 80% ESO samples on the other was observed. Disperse phase domains in 40% ESO systems are about one order of magnitude smaller than disperse phase domains in the samples with higher ESO content. Also, in the 40% ESO system image, some of the disperse domains seem to have been pulled out of the matrix, leaving an empty hole, and some others appear as protuberance. This feature was not observed in the 60 and 80% ESO systems. This difference in the morphology is expected to produce an important change in the fracture behavior of the copolymers.

Fracture Behavior

Typical fracture load-displacement curves under three-point bending are shown in Fig. 4 for all copolymers. F4 Curves are linear with an abrupt load fall and fracture surfaces are macroscopically brittle. Corresponding toughness values, in terms of K_{IC}, are depicted in Table 1. K_{IC} T1 value for 100% ESO was found to be near the double of that of 0%ESO. Figure 5 shows TOM micrographs taken F5 under bright field (without cross-polarizers) and polarized light of the fresh zones generated in four-point bending tests. Under cross-polarized light birefringence is seen, which typically indicates matrix shear yielding or shear bands. Optical micrographs show a tendency of the stress

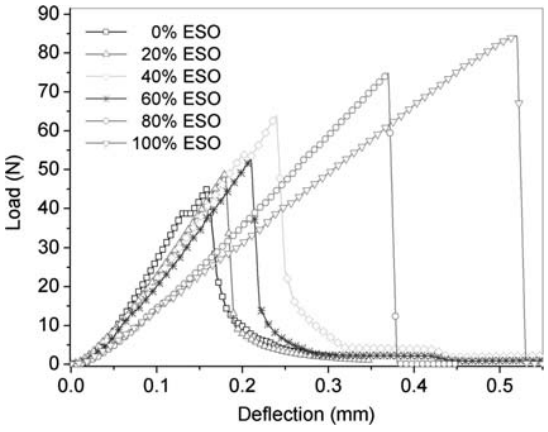

FIG. 4. Load-displacement curves obtained in the three-point bending tests for SEN specimens. [Color figure can be viewed in the online issue, which is available at wileyonlinelibrary.com.]

TABLE 1. K_{IC} values for the DGEBA-ESO/MTHPA systems as a function of the ESO content[a].

ESO%	K_{IC} (MPa·m$^{1/2}$)
0	0.557 (0.113) a
20	0.637 (0.070) a,b
40	0.765 (0.108) b,c
60	0.706 (0.049) a,b
80	0.916 (0.062) c
100	1.067 (0.113) d

Values in parenthesis indicate standard deviations.

[a] Different letters indicate that K_{IC} values are significantly different at $p < 0.05$.

field associated to deformation to increase with ESO content, with a discontinuity in 40% ESO. The comparison of the birefringence zone size shows that 40% ESO material experienced a lower degree of plastic deformation than 20% ESO, although higher fracture toughness was obtained herein (Table 1), contradicting to a well-known fact that a larger birefringent zone often corresponds to a higher fracture toughness. Similar findings were reported by Le et al. [26] who rightly pointed out that this may be due to a more localized deformation process involving small dispersed particles (it should be recalled here that at 40% ESO content phase separation occurred). Consistently with TOM findings, it was found that K_{IC} showed a general increasing trend with ESO content (Table 1). Nevertheless, a discontinuity in the K_{IC} values was observed between 40 and 60% ESO. This observation suggests that besides phase separation occurring between 40 and 80% of ESO content, a phase inversion could be taking place when the ESO content is raised from 40 to 60%.

Depth-sensing indentation tests performed on both phases of samples with 40 and 60% ESO gave conclusive evidence of the phase inversion. The obtained curves and *in situ* SPM images of 40 and 60% ESO samples are shown in Figs. 6 and 7, respectively. For 40% systems, the load-displacement curve of the continuous phase has a higher slope (i.e., is more rigid), indicating a lower ESO content, than the disperse phase. This difference in the modulus is reflected by the reduced modulus (Er), and the hardness, indicated in the inset table for each phase. The opposite was observed for the 60% ESO systems, but a slighter difference between both phases was found in this case. F7 F6

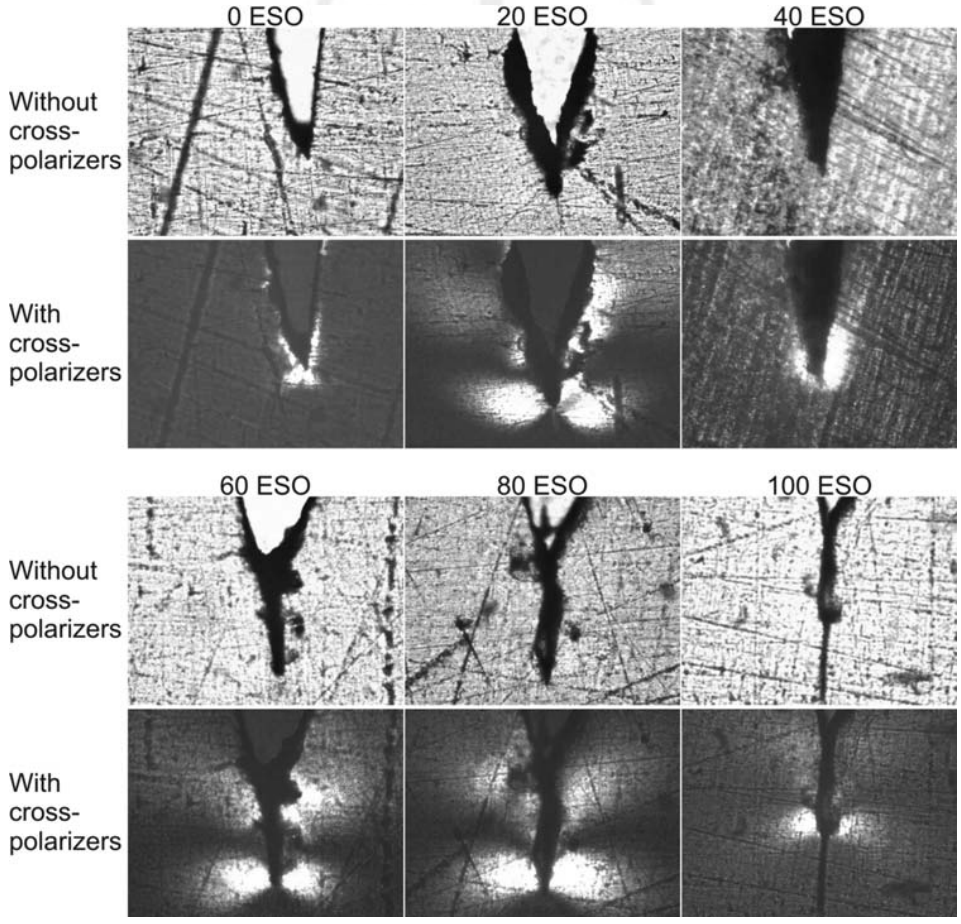

FIG. 5. TOM images of the damage zone surrounding the crack tip with and without cross-polarizers, with a magnification of 200×. [Color figure can be viewed in the online issue, which is available at wileyonlinelibrary.com.]

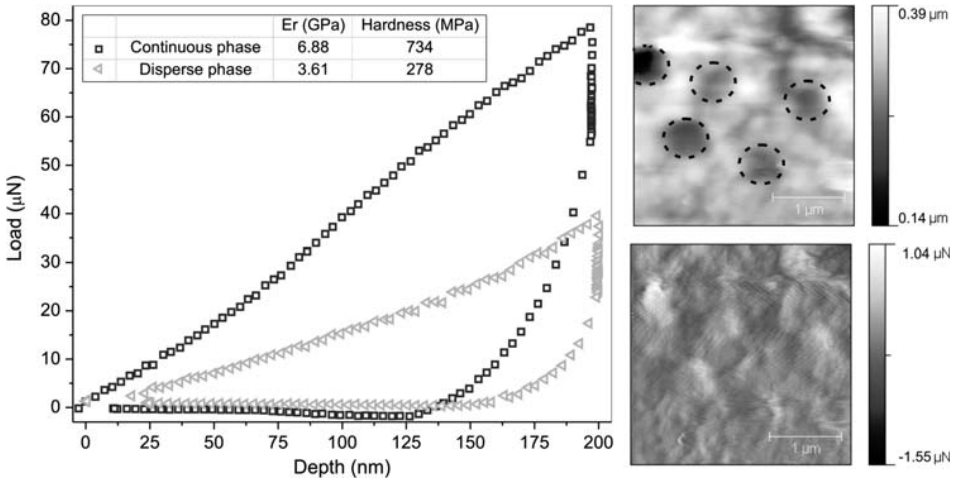

FIG. 6. Load-displacement curves for the 40% ESO continuous and disperse phase, and SPM images (up: topography; down: gradient) of the test sample. The disperse phase domains are indicated by a dashed-line circle in the topography image. [Color figure can be viewed in the online issue, which is available at wileyonlinelibrary.com.]

According to these results, it is clear that the disperse phase is the less rigid one for the 40% ESO polymers, contrary to what was observed for the 60% ESO systems, where the disperse phase is more rigid than the continuous one.

On this basis, copolymers with ESO content up to 40% are systems with a rigid matrix which yield stress diminished due to the plasticizing effect of ESO. According to Kinloch et al. [21, 27] shear yielding deformation is the main mechanism of energy dissipation during fracture of epoxy networks, which is favored by a low σ_y. In addition, in 40% ESO system there is a softer dispersed phase. As it is well known, the presence of a more ductile disperse phase [21, 28], or dispersed microvoids [29] in a stiffer matrix can promote the plastic deformation of the matrix increasing the material toughness. The presence of a softer disperse phase was also used to justify the increase in K_{IC} values of DGEBF-ESO/MTHPA/1MI systems when replacing 30% of DGEBF by ESO [19]. Conversely, for copolymers with 60 and 80% ESO only the decrease of σ_y with the increase in ESO content could be responsible of the increasing toughness of high ESO content copolymers. These explanations are reflected in Fig. 8, in which K_{IC} is plotted against σ_y (σ_y values were reported elsewhere [20]. In spite of having a higher σ_y value, 40% ESO systems displayed a higher toughness than 60% ESO systems because the effect of the softer disperse phase in the first one that does not take place in the latter. F8

AFM inspection of fresh zones ahead of the crack tip (DN-4PB tests) gives a better insight to failure

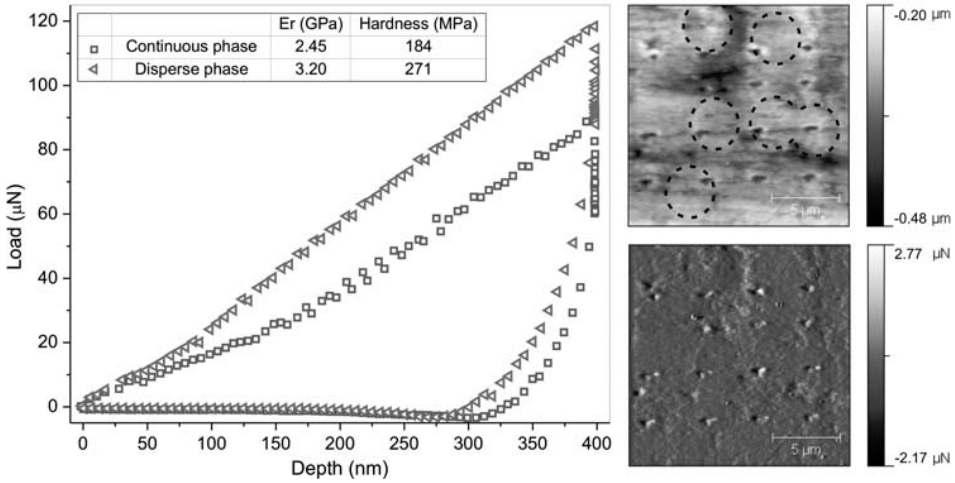

FIG. 7. Load-displacement curves for the 60% ESO continuous and disperse phase, and SPM images (up: topography; down: gradient) of the test sample. The disperse phase domains are indicated by a dashed-line circle in the topography image. [Color figure can be viewed in the online issue, which is available at wileyonlinelibrary.com.]

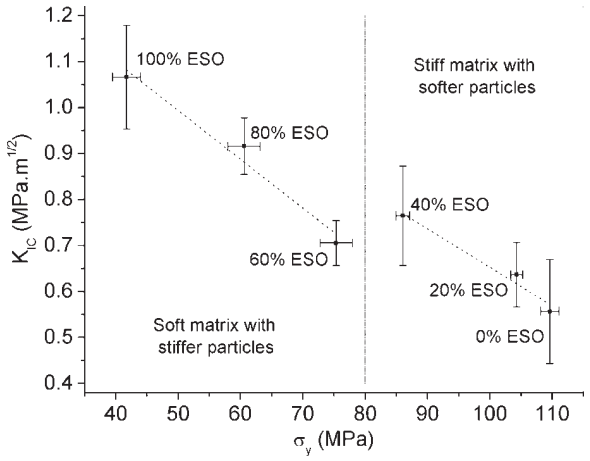

FIG. 8. Fracture toughness as a function of the yield stress for the different ESO contents. Standard deviations (both for K_{IC} and σ_y) are indicated by bars.

mechanisms (Fig. 9). In 40% ESO system, distortion of the softer particles ahead of the crack tip and blunting of the crack are clearly seen. It is therefore concluded that the matrix underwent shear yielding, that is, plastic deformation prior to fracture [24, 28, 30]. Contrary, in 60% ESO samples is evident that the crack advanced through the soft matrix surrounding the rigid particles, and no plastic deformation is observed. This change in failure mechanism corresponds to the inversion of phases described above. F9

Optical Properties

A remarkable aspect of the copolymers is that, in spite of the described phase separation, most of copolymers were transparent except for that containing 60% ESO which exhibited increased opacity. As the continuous and

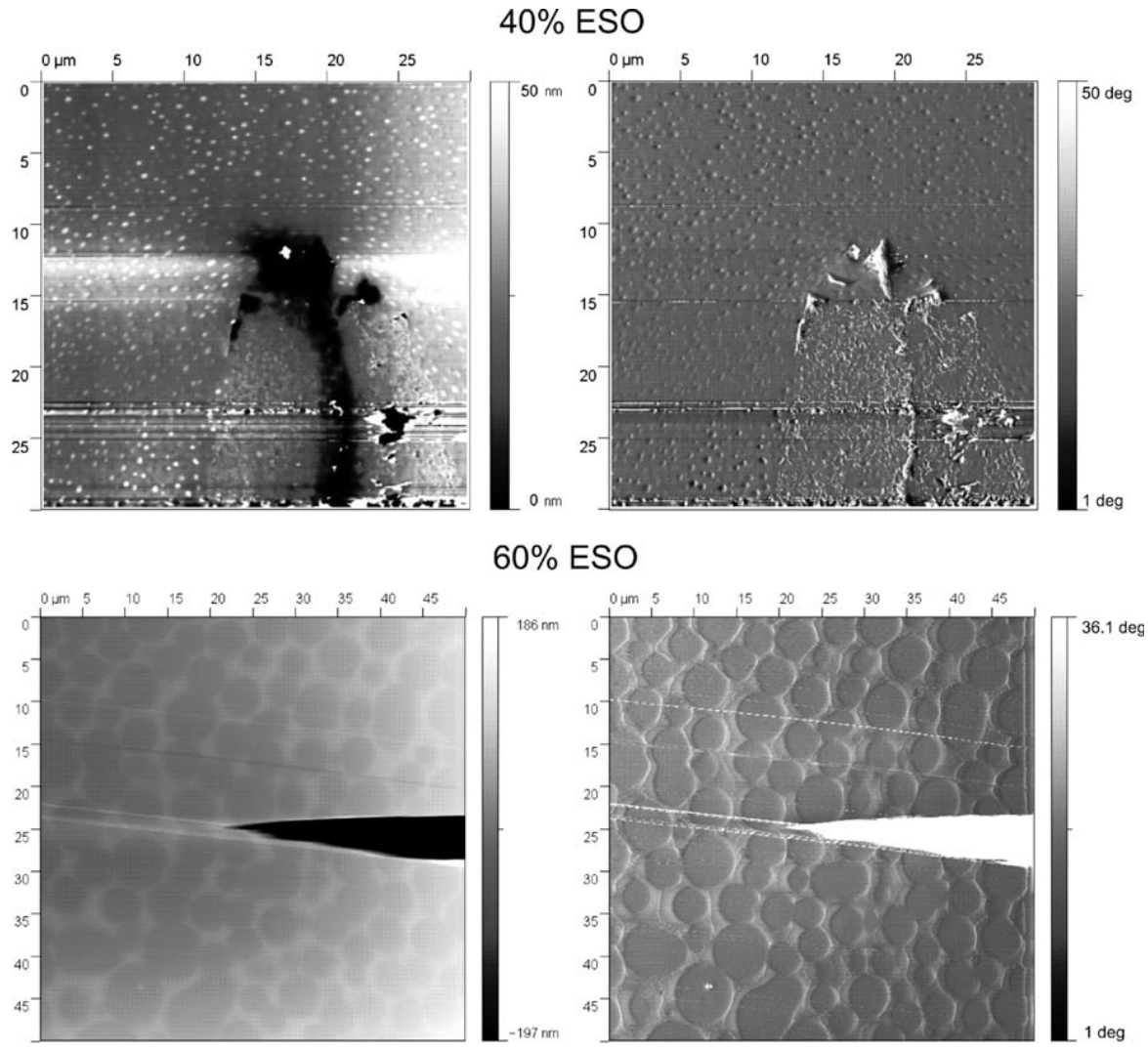

FIG. 9. AFM images of the crack tip surrounding zone of specimens with 40 and 60% ESO. Height (left) and phase (right) images. [Color figure can be viewed in the online issue, which is available at wileyonlinelibrary.com.]

DOI 10.1002/pen

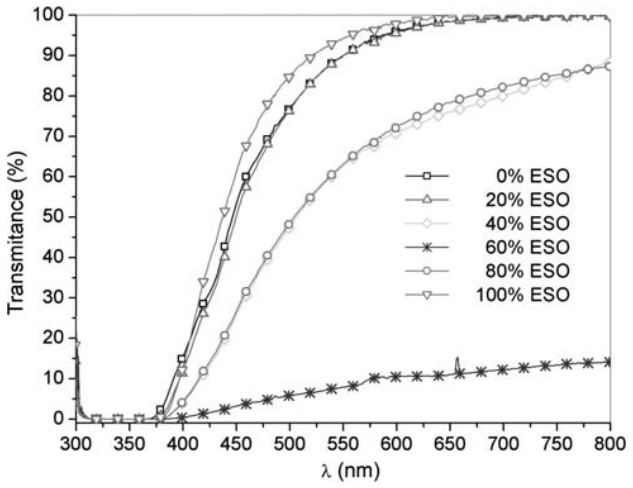

FIG. 10. DGEBA-ESO/MTHPA copolymers visible light transmittance across 150–170-μm thick samples. [Color figure can be viewed in the online issue, which is available at wileyonlinelibrary.com.]

TABLE 2. Average transmittance in the 400–800 nm range.

ESO %	Transmittance (%)
0	84.2
20	83.6
40	61.8
60	9.0
80	63.0
100	87.3

the dispersed phases have similar compositions [20], it is postulated that both phases have similar refractive indexes, and thus, copolymers showed little or no light scattering. If compatibility between phases is poor, light dispersion or reflection at the two-phase interface occurs, and the light transmittance is low.

Transmittance of visible light was measured to quantitatively analyze the transparency of the copolymers, and the results are shown in Fig. 10. A decrease of the transmittance is observed for lower wavelength, regardless the ESO content, and was associated with the brownish color acquired by the samples during the high temperature curing step, due to the presence of the imidazole ring [31]. Copolymers with 40 and 80% ESO displayed a relative high value of transparency, in spite of the biphasic morphology revealed by AFM analysis (Fig. 3). The same conclusion arises from the analysis of the values of the average transmittance, summarized in Table 2. In contrast, 60% ESO sample showed a lower light transmittance in the range of 300–800 nm when compared to the other systems. This result might not be associated with differences in thickness since average values were in the range of 150–170 μm. A plausible explanation for this observation is the difference in the morphologies. 60% ESO copolymers displayed a higher volume fraction of disperse phase than 40 and 80% ESO systems. This, combined with the large size of the disperse phase domains, could lead to a significant light scattering, even with small differences in the refractive index of both phases. In addition, all the copolymers showed a low UV light transmission, which is an advantage for the application of these materials as protective coatings. The macroscopic aspect of the samples used to assess the transparency can be observed in Fig. 11. In this photograph, little or no opalescence is observed, even for the 60% ESO sample, giving a clear evidence of the potential of these materials for optical applications.

CONCLUSION

ESO was proved to be a good alternative to replace (at least partially) a synthetic commercial epoxy resin in a formulation to obtain thermosetting polymer, contributing to transform a vegetable oil into a higher added value product. The properties of the copolymers obtained using the epoxidized oil were comparables to those of the synthetic resin, and the fracture toughness was greatly improved, mainly due to the lower yield stress of the cured ESO. The only exception to this trend was due to the phase inversion observed when the ESO content was raised from 40% to 60, which led to a decrease of the K_{IC} value, in spite of the lower yield stress of the 60% ESO copolymer. It is noteworthy that most of the formulations present high values of transparency, which would make them suitable for some optical applications such as matrices for composites used in optoelectronic devices, or protective coatings and paints.

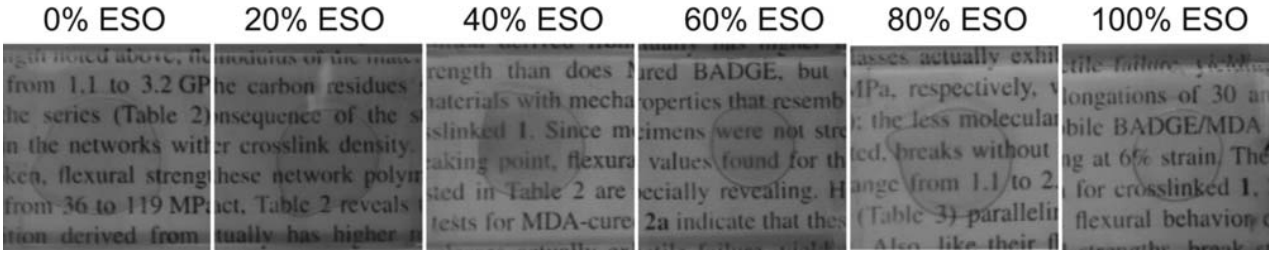

FIG. 11. Macroscopic aspect of the copolymer samples used to assess the visible light transmittance. [Color figure can be viewed in the online issue, which is available at wileyonlinelibrary.com.]

ACKNOWLEDGMENT

This article is dedicated In Memoriam of Prof. Iñaki Mondragon Egaña.

NOMENCLATURE

Abbreviations and Symbols

1MI	1-Methyl imidazole
A	Crack length in the fracture specimen (cm)
AFM	Atomic force microscopy
B	Fracture specimen width (cm)
DGEBA	Diglycidyl ether of bisphenol A
DGEBF	Diglycidyl ether of bisphenol F
DN-4PB	Double-notch four-point-bending
E'	Storage modulus (GPa)
EEW	Epoxide equivalent weight
ECO	Epoxidized castor oil
ELO	Epoxidized linseed oil
Er	Reduced modulus (GPa)
ESO	Epoxidized soybean oil
EVO	Epoxidized vegetable oil
K_{IC}	Critical stress intensity factor in plane strain ($MPa \cdot m^{1/2}$)
MTHPA	Methyl tetrahydrophtalic anhydride
p	Confidence interval threshold for the Tukey test
P	Maximum load in the fracture tests (kN)
PVC	Poly(vinyl chloride)
R	Universal gas constant [=8314 l kPa/(K mol)]
SEN	Single edge notch
SPM	Scanning probe microscopy
T_g	Glass transition temperature (°C)
TOM	Transmission optical microscopy
UV	Ultra-violet
W	Fracture specimen height (cm)
α	ANOVA significance level
v	Crosslinking density (mol/m^3)
σ_y	Compressive yield strength (MPa)

REFERENCES

1. X.S. Sun and R.P. Wool, *Bio-Based Polymers and Composites*, Elsevier, Acad. Press, Amsterdam [u.a.], (2005).
2. A. Corma, S. Iborra, and A. Velty, *Chem. Rev.* **107**, 2411 (2007).
3. A. Gandini, *Green Chem.* **13**, 1061 (2011).
4. L. Shen, E. Worrell, and M. Patel, *Biofuels Bioprod. Bioref.* **4**, 25 (2010).
5. G.-Q. Chen and M.K. Patel, *Chemical Reviews* **112**, 2082 (2012).
6. N. Boquillon and C. Fringant, *Polymer* **41**, 8603 (2000).
7. M.A.R. Meier, J.O. Metzger, and U.S. Schubert, *Chem. Soc. Rev.* **36**, 1788 (2007).
8. G. Lligadas, J.C. Ronda, M. Galià, and V. Cádiz, *Biomacromolecules* **11**, 2825 (2010).
9. L. Montero de Espinosa and M.A.R. Meier, *Eur. Polym. J.* **47**, 837 (2011).
10. United States Department of Agriculture, *World Agricultural Outlook Board* **28** (2012). AQ3
11. R.P. Wool and S.N. Khot, in *ASM Handbook Volume 21, Composites, 10 ed.*, S.L. Donaldson and D.B. Miracle, Eds., ASM International, **184** (2001). AQ4
12. F. Okieimen, O. Bakare, and C. Okieimen, *Ind. Crop. Prod.* **15**, 139 (2002).
13. S. Warwel and M. Rüsch gen. Klaas, *J. Mol. Catal. B-Enzym.* **1**, 29 (1995).
14. M. Rüsch gen. Klaas and S. Warwel, *Ind. Crop. Prod.* **9**, 125 (1999).
15. I. Hilker, D. Bothe, J. Prüss, and H.-J. Warnecke, *Chem. Eng. Sci.* **56**, 427 (2001).
16. C. Bueno-Ferrer, M.C. Garrigós, and A. Jiménez, *Polym. Degrad. Stab.* **95**, 2207 (2010).
17. A.E. Gerbase, C.L. Petzhold, and A.P.O. Costa, *J. Am. Oil Chem. Soc.* **79**, 797 (2002).
18. S.-J. Park, F.-L. Jin, and J.-R. Lee, *Mater. Sci. Eng. A-Struct.* **374**, 109 (2004).
19. H. Miyagawa, M. Misra, L.T. Drzal, and A.K. Mohanty, *Polym. Eng. Sci.* **45**, 487 (2005).
20. F.I. Altuna, L.H. Espósito, R.A. Ruseckaite, and P.M. Stefani, *J. Appl. Polym. Sci.* **120**, 789 (2011).
21. A.J. Kinloch, S.J. Shaw, D.A. Tod, and D.L. Hunston, *Polymer* **24**, 1341 (1983).
22. D. Ratna, *Polym. Int.* **50**, 179 (2001).
23. F.-L. Jin and S.-J. Park, *Mater. Sci. Eng. A-Struct.* **478**, 402 (2008).
24. M.L. Arias, P.M. Frontini, and R.J. Williams, *Polymer* **44**, 1537 (2003).
25. M.L. Auad, S.R. Nutt, V. Pettarin, and P.M. Frontini, *Express Polym. Lett.* **1**, 629 (2007).
26. Q.-H. Le, H.-C. Kuan, J.-B. Dai, I. Zaman, L. Luong, and J. Ma, *Polymer* **51**, 4867 (2010).
27. A.J. Kinloch, S.J. Shaw, and D.L. Hunston, *Polymer* **24**, 1355 (1983).
28. P.M. Stefani, S.M. Moschiar, and M.I. Aranguren, *J. Appl. Polym. Sci.* **82**, 2544 (2001).
29. Y. Huang and A.J. Kinloch, *Polymer* **33**, 1330 (1992).
30. A.J. Kinloch and J.G. Williams, *J. Mater. Sci.* **15**, 987 (1980).
31. Y.R. Ham, S.H. Kim, Y.J. Shin, D.H. Lee, M. Yang, J.H. Min, and J.S. Shin, *J. Ind. Eng. Chem.* **16**, 556 (2010).